Signal Processing 110 (2015) 244–249

Contents lists available at ScienceDirect

Signal Processing

journal homepage: www.elsevier.com/locate/sigpro

A hypothesis independent subpixel target detector for hyperspectral Images

Bo Du [a], Yuxiang Zhang [b], Liangpei Zhang [c], Lefei Zhang [a,*]

[a] School of Computer, Wuhan University, P.R. China
[b] The School of Remote Sensing and Information Engineering, Wuhan University, P.R. China
[c] The State Key Laboratory of Information Engineering in Surveying, Mapping, and Remote Sensing, Wuhan University, P.R. China

ARTICLE INFO

Article history:
Received 4 May 2014
Received in revised form
26 July 2014
Accepted 12 August 2014
Available online 27 August 2014

Keywords:
Hyperspectral image
Hypothesis independent
Maximum likelihood method
Matched subspace detector
Subpixel target detection

ABSTRACT

In previous work, the statistical characteristics of the background or the noise under H_0 hypothesis are similar as that under H_1 hypothesis. Accordingly, the parameters under both hypotheses are estimated by the maximum likelihood method and finally a generalized likelihood ratio test based detector is developed, such as the matched subspace detector. Unfortunately, this kind of statistical similarity for both hypotheses may be changing, which is directly related to the unknown beforehand target fill factor. A hypothesis independent method is proposed to solve this problem, which uses different approaches to estimate the parameters for different hypotheses. Experiments on simulated data and real hyperspectral image demonstrate the ability of this proposed detector for subpixel target detection.

1. Introduction

As we know that, any target detection application seeks to identify a relatively small number of objects with fixed shape or spectrum in a scene. However, hyperspectral target detection is much different from other target detection methods [1], as hyperspectral image (HSI) conveys abundant spectral information [2–4]. Furthermore, due to the low spatial resolution of the sensor, targets are likely to be embedded in a single pixel, and subpixel targets detection becomes a research focus [5,6].

The subspace model is usually employed for the subpixel target detection [7–10]. The matched subspace detector (MSD) is a typical subpixel targets detector. MSD employs the linear mixture model (LMM) to model the background or target pixel which corresponds to the H_0 or H_1 hypothesis, and uses the maximum likelihood method (MLE) to estimate the unknown parameters for two hypotheses [11–13]. This work assumes that the background power under H_0 hypothesis remains the same as that under H_1 hypothesis. However, in practice, it is usually the case that the background power will change with the appearance of target, and the background variance is directly related to the target fill factor which is the percentage of the pixel area occupied by the target [14]. Based on this point, a hypothesis independent method named HMSD is presented in this paper which is based on the matched subspace detector, and where the noise power is estimated using different methods. As the number of target pixel in the HSI is much limited, it is convenient to use the target-free data to calculate the noise variance under the null hypothesis. The noise under the alternative hypothesis is unknown and can be estimated using the MLE method. The detailed information about the method is discussed in the following.

2. HMSD

The test pixel in the hyperspectral image is modeled in terms of the target subspace and background subspace

* Corresponding author.
E-mail address: zhanglefei@whu.edu.cn (L. Zhang).

http://dx.doi.org/10.1016/j.sigpro.2014.08.018
0165-1684/

respectively. The competing hypotheses for a mixed pixel are:

$$\begin{aligned}\mathbf{x}&=\mathbf{B}\mathbf{a}_{b0}+\sigma_0\mathbf{n}, \quad \text{Under } H_0\\ \mathbf{x}&=\mathbf{S}\mathbf{a}_t+\mathbf{B}\mathbf{a}_{b1}+\sigma_1\mathbf{n}, \quad \text{Under } H_1\end{aligned} \tag{1}$$

The notations are listed in Table 1. The background subspace can be defined by the first Q eigenvectors of the image covariance matrix corresponding to the larger eigenvalues.

If we estimate the noise variance σ_0^2 with the target-free data and estimate the remaining unknown parameters ($\mathbf{a}_{b0}$, $\mathbf{a}_{b1}$, $\mathbf{a}_t$, σ_1^2) using the MLE technique, thus a new detection statistic can be developed by the generalized likelihood ratio test (GLRT) approach. To do this, we calculate the likelihood equations for the null and alternative hypothesis as

$$\begin{aligned}L(\mathbf{x}|H_0)&=(2\pi\sigma_0{}^2)^{-L/2}\times\exp\left\{-\tfrac{1}{2\sigma_0{}^2}(\mathbf{x}-\mathbf{B}\mathbf{a}_{b0})^{\mathrm{T}}(\mathbf{x}-\mathbf{B}\mathbf{a}_{b0})\right\}\\ L(\mathbf{x}|H_1)&=(2\pi\sigma_1{}^2)^{-L/2}\times\exp\left\{-\frac{1}{2\sigma_1{}^2}(\mathbf{x}-\mathbf{S}\mathbf{a}_t-\mathbf{B}\mathbf{a}_{b1})^{\mathrm{T}}\times(\mathbf{x}-\mathbf{S}\mathbf{a}_t-\mathbf{B}\mathbf{a}_{b1})\right\}\end{aligned} \tag{2}$$

Taking the derivative of the logarithm of (2) with respect to each of the unknown parameters and setting them equal to zero allows us to arrive at the MLE-based abundance estimation

$$\begin{aligned}\widehat{\mathbf{a}}_{b0}&=(\mathbf{B}^{\mathrm{T}}\mathbf{B})^{-1}\mathbf{B}^{\mathrm{T}}\mathbf{x}\\ \widehat{\mathbf{a}}_{b1}&=(\mathbf{A}^{\mathrm{T}}\mathbf{A})^{-1}\mathbf{A}^{\mathrm{T}}\mathbf{x}\\ \widehat{\mathbf{a}}_t&=(\mathbf{C}^{\mathrm{T}}\mathbf{C})^{-1}\mathbf{C}^{\mathrm{T}}\mathbf{x}\end{aligned} \tag{3}$$

And the noise variance estimation for the alternative hypothesis is

$$\widehat{\sigma}_1^2=\frac{1}{L-J}||\mathbf{P}_E^{\perp}\mathbf{x}||^2=\frac{1}{L-J}||\mathbf{x}_E^{\perp}||^2 \tag{4}$$

where $\mathbf{A}=\mathbf{P}_S^{\perp}\mathbf{B}$, $\mathbf{C}=\mathbf{P}_B^{\perp}\mathbf{S}$, and $\mathbf{E}=[\mathbf{B},\mathbf{P}_B^{\perp}\mathbf{S}]$. $\mathbf{P}_E=\mathbf{E}(\mathbf{E}^T\mathbf{E})^{-1}\mathbf{E}^T$, $\mathbf{P}_E^{\perp}=\mathbf{I}-\mathbf{P}_E$, and $\mathbf{x}_E^{\perp}=\mathbf{P}_E^{\perp}\mathbf{x}$. $\mathbf{P}_S$ and $\mathbf{P}_B$ are the orthogonal projection matrices onto the target and background subspaces, and $\mathbf{P}_E$ is the orthogonal projection matrix onto the concatenation of the background and target subspaces with background subspace effect eliminated in target subspace. Then, the GLR is given by

$$\frac{p(\mathbf{x};\widehat{\mathbf{a}},\widehat{\sigma}_1{}^2|H_1)}{p(\mathbf{x};|H_0)}=\frac{\left\{2e^{(L-J)/L}\pi(L-J)^{-1}||\mathbf{x}_E^{\perp}||^2\right\}^{-L/2}}{(2\pi\sigma_0{}^2)^{-L/2}\mathrm{e}^{\left\{\frac{||\mathbf{x}_B^{\perp}||^2}{2\sigma_0{}^2}\right\}}} \tag{5}$$

Using some algebra, the GLRT-based detector named HMSD is given by the following statistical test

$$D_{HMSD}(\mathbf{x})=\frac{||\mathbf{x}_B^{\perp}||^2}{L\sigma_0{}^2}-\ln\frac{||\mathbf{x}_E^{\perp}||^2}{(L-J)\sigma_0{}^2}-\frac{L-J}{L} \tag{6}$$

where J=P+Q, $||\mathbf{x}_B^{\perp}||^2=||\mathbf{x}_t||^2+||\mathbf{x}_E^{\perp}||^2$, and $\mathbf{x}_t=\mathbf{P}_C\mathbf{x}$. We can rewrite the proposed detector in the following form

$$D_{HMSD}(\mathbf{x})=\frac{||\mathbf{x}_t||^2}{L\sigma_0{}^2}+\frac{||\mathbf{x}_E^{\perp}||^2}{L\sigma_0{}^2}-\ln\frac{||\mathbf{x}_E^{\perp}||^2}{(L-J)\sigma_0{}^2}-\frac{L-J}{L} \tag{7}$$

We can see from (7) that the detection quality depends on the relation between the target contribution (the first term) and the background power change contribution (the second and third terms). We can adjust the background power change sensitivity of detector with respect to the target presence sensitivity using a factor m. Varying the factor m we can adapt the background power change to the detection performance. We can introduce the factor of signal detection sensitivity m and rewrite the proposed detector in the following form

$$D_{HMSD}(\mathbf{x})=\frac{||\mathbf{x}_t||^2}{L\sigma_0{}^2}+m\left\{\frac{||\mathbf{x}_E^{\perp}||^2}{L\sigma_0{}^2}-\ln\frac{||\mathbf{x}_E^{\perp}||^2}{(L-J)\sigma_0{}^2}\right\}-\frac{L-J}{L} \tag{8}$$

For simplicity, we actually rewrite it in the following form:

$$D_{HMSD}(\mathbf{x})=\frac{\mathrm{m}||\mathbf{x}_t||^2}{L\sigma_0{}^2}+\frac{||\mathbf{x}_E^{\perp}||^2}{L\sigma_0{}^2}-\ln\frac{||\mathbf{x}_E^{\perp}||^2}{(L-J)\sigma_0{}^2} \tag{9}$$

In this paper, the noise variance under the null hypothesis was estimated by a local median filter method. A noise matrix is first estimated by subtracting the target-free image matrix with median filter from the original target-free image matrix, which is similar as that in Maximum Noise Fraction (MNF) method [15,16]. Then, the noise variance can be calculated from this noise matrix. However, in practice, the target-free image cannot obtain, in view of the limited number of targets, it can be replaced with the whole image. According to the aforementioned descriptions, the HMSD algorithm for hyperspectral target detection can be expressed as Table 2.

Table 1
Notations in HMSD model.

notation	Meaning	Size
$\mathbf{x}$	pixel spectrum vector	L × 1
$\mathbf{S}$	target subspace	L × P
$\mathbf{B}$	background subspace	L × Q
$\mathbf{a}_{b0}$, $\mathbf{a}_{b1}$	background abundance for two hypotheses	L × 1
$\mathbf{a}_t$	target abundance	L × 1
$\mathbf{n}$	multivariate normal noise	L × 1
σ_0^2, σ_1^2	variance for two hypotheses	

Table 2
The HMSD algorithm.

Input: a hyperspectral image, target prior spectra, and parameters *m and* Q*;*

Processing:
Obtain the median filtered image, and then obtain the noise image;
Calculate the noise variance σ_0^2;
Calculate the image covariance matrix, and obtain the first Q eigenvectors corresponding to the larger eigenvalues as **B**;
Compute the detection statistics via (9)
Output: maps of the detection statistics of each pixel.

3. Experiments

To test the effectiveness of the HMSD, series of experiments are conducted on the synthetic and real hyperspectral datasets. The performance of HMSD is compared with MSD and other state-of-the art target detectors including the sparse representation detector (SRD) [17] and the background self-learning method (BSL) [18]. The experimental platform is a PC with Inter(R) Core(TM) i3, 2.20 GHz, 4 G memory and 64 bit windows 7. All algorithms are implemented by Matlab 2010a.

The synthetic dataset was generated by four kinds of plants as background materials and soil as target materials from the ENVI's spectral library showed in Fig.1. The spectral signature has 100 bands. First, we obtain the background image by a linear combination of background endmember spectra and the additive noise modeled by a multivariate normal distribution. The abundances for the background endmembers are random set with two constraints that the sum of abundances is 1 and the abundances are nonnegative. The SNR of the noise is respectively set as 5, 10, 15, 20, 25, and 30. Then we gain the target present image by adding the target endmember to particular pixels in the background image according to a certain target fill factor f. f is set as 0.1, 0.2, 0.3, 0.4, 0.5, 0.6, 0.7, 0.8, 0.9, and 1. For each pair of SNR and f, we add the target endmember to 100 particular pixels.

A target implant method [19] is used in this paper. Based on a linear mixing model, a synthetic sub-pixel target with spectrum $\mathbf{z}$ is generated by fractionally implanting a desired target with spectrum $\mathbf{t}$ in a given pixel of the background with spectrum $\mathbf{b}$, as follows [20]

$$\mathbf{z} = f \cdot \mathbf{t} + (1-f) \cdot \mathbf{b} \tag{10}$$

We can regard the known endmembers matrix ($\mathbf{B}$ and $\mathbf{S}$) and noise variance σ_0^2 as a priori. Thus the simulated data is convenient to quantitatively measure the influence of the presence of the targets to the noise power. To test the ability of the factor m, we can adjust it and then compare the detection efficiency of HMSD and MSD.

Fig.2 is a real HIS data which was collected by the Hyperspectral Digital Image Collection Experiment (HYDICE) sensor. 162 bands of the data are retained. The image scene is 150×150 pixels. This dataset is an urban scene in which there are nine vehicles, including 19 target pixels as targets to be detected.

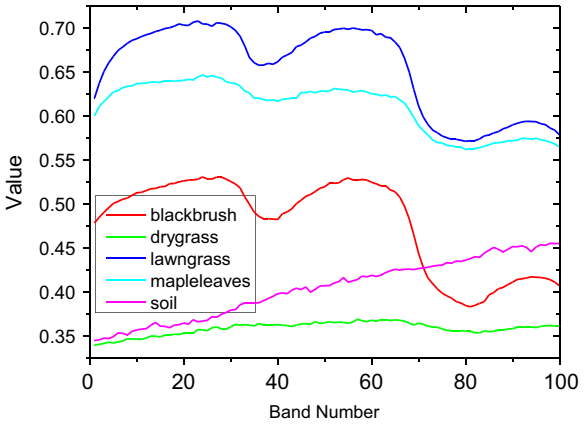

Fig. 1. Endmembers spectrum.

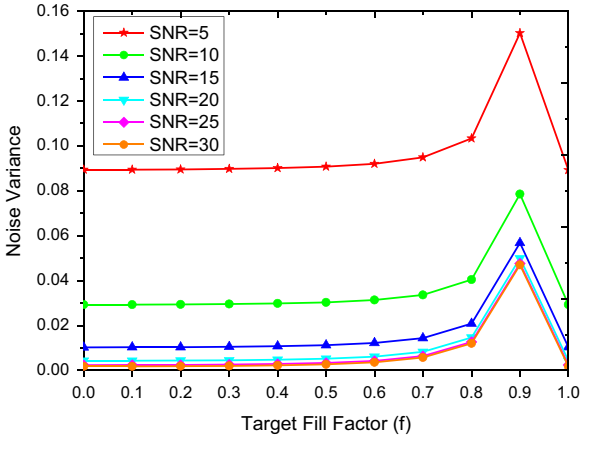

Fig. 3. The influence of the targets to the noise power.

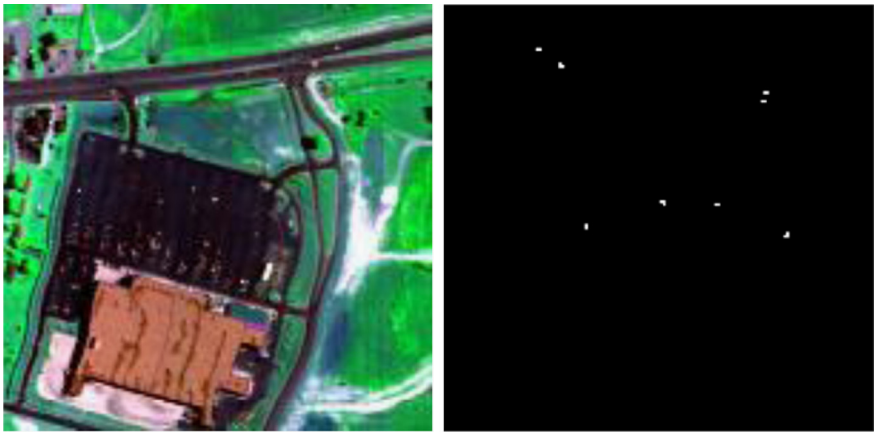

Fig. 2. The HYDICE data and ground truth.

Firstly, we examine the influence on the noise variance when the targets with different fill factors are added to the background image based on the synthetic dataset. The size of the local square window for median filter can be set as 5×5. The noise variance curves with different SNR and target fill factor are shown in Fig.3. From the results, we can see that the presence of targets triggers an increase in the noise power in general. Specially, the noise power will increase with f until f reaches to 0.9. And when the background amount in the pixel decreases to zero, the noise power presents a severe decrease.

Then we demonstrate how the detection performance of HMSD is affected by the signal detection sensitivity factor m. There is no automatically adjusting method for m now. The detection probability (pd) curves for the synthetic images with specific values of SNR and different target fill factors are shown in Fig.4. The detection probability (pd) is estimated at a specific threshold where the number of the detected target pixels reaches the number of the real target pixels. The results show that the detection performance decreases gradually and then becomes stable with the factor m. And for the image with a small target fill factor, it is hardly useful to adjust the signal detection sensitivity factor m. So we may choose a lower value of m for target detection. For the real HYDICE data, the result is shown via the area under the receiver operating characteristic (ROC) curves [21]. Fig. 5 reveals that the probability of detection increases with m until it reaches 16 and then slowly decreases with m. The results difference for both datasets may be resulted from the different background endmembers method.

Finally, the detection performance of HMSD is evaluated with three different algorithms. The signal detection sensitivity factor m is set as the optimal value according to the above results. As there is more prior information for MSD and HMSD than that for SRD and BSL in the synthetic data, we just compare HMSD with MSD. The experimental results for the synthetic images with SNR=5 and 20 are provided through Fig. 6. The results show that HMSD significantly outperforms MSD at any target fill factor f. For the real HYDICE data, the detection performance is shown via the ROC curves, the area under the ROC curve (AUC), and the time consumption, as shown in Fig. 7 and Table 3. The results demonstrate that the ROC curve of HMSD is closest to the left-and-up corner, the area under the ROC curve of HMSD is the largest, and the time consumption is much small, which reveals the effectiveness of HMSD in detecting the subpixel targets.

4. Summary and future work

The statistical features of the noise and the background for H_0 and H_1 hypotheses may be different from each other. The hypothesis independent method is introduced to solve this problem, where the noise power is only known under the null hypothesis and the structured background power can be regulated by the factor of signal detection sensitivity m. The HMSD was demonstrated as an effective way of subpixel target detection in hyperspectral data. Experiments on different subpixel hyperspectral datasets present

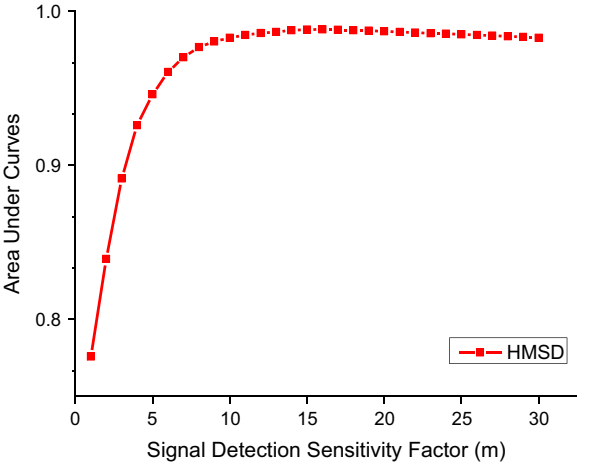

Fig. 5. The influence of m to detection probability.

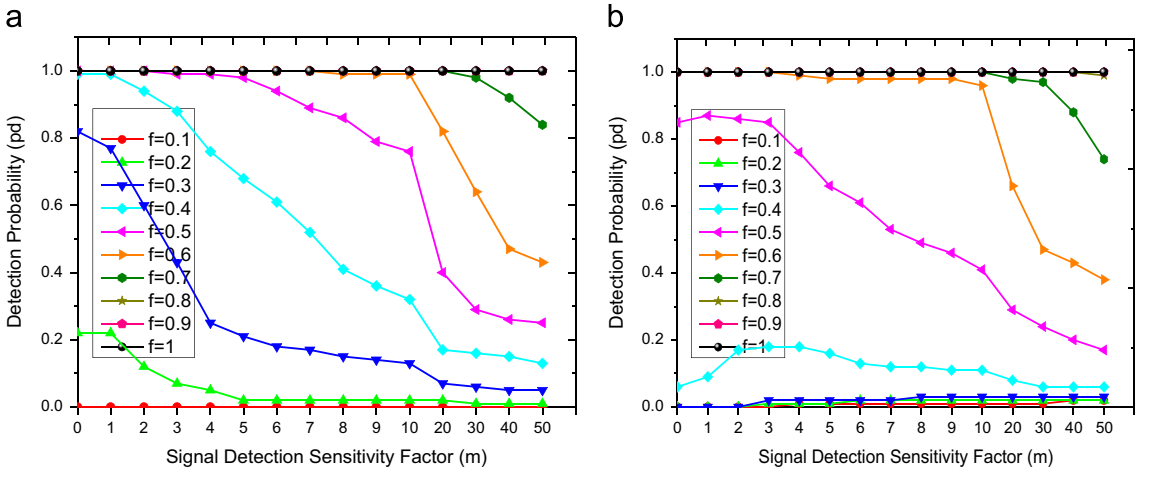

Fig. 4. The influence of parameter m to detection probability. (a) SNR=5 and (b) SNR=20.

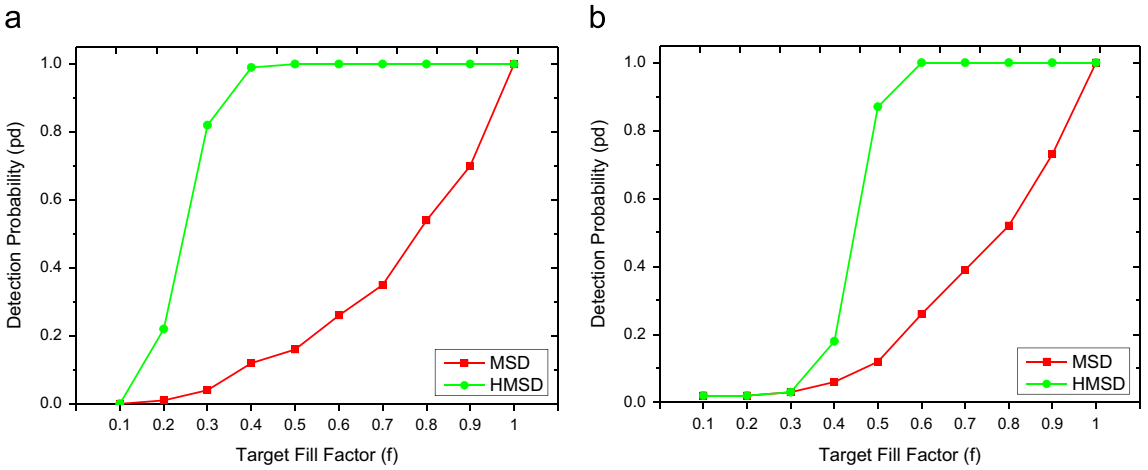

Fig. 6. Detection performance for synthetic data. (a) SNR=5 and (b) SNR=20.

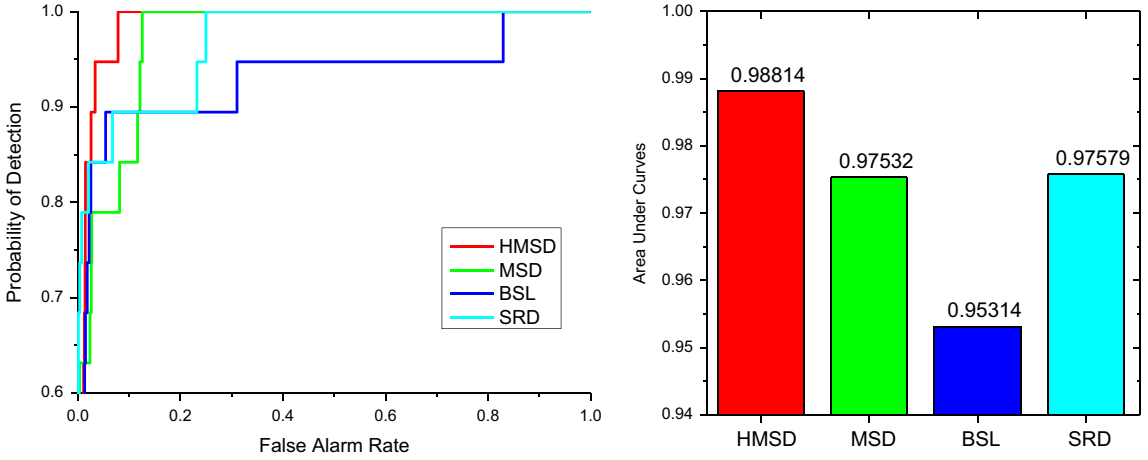

Fig. 7. Detection performance for HYDICE data.

Table 3
The time consumption for four algorithms.

	HMSD	MSD	BSL	SRD
Time(s)	4.98	2.80	641.70	97.40

the superiority of HMSD. Our future research will investigate different noise estimation methods.

Acknowledgment

The authors would like to thank the handing editor and the anonymous reviewers for their careful reading and helpful remarks, which have contributed in improving the quality of this paper. This paper is supported in part by the National Basic Research Program of China (973 Program) under Grant 2012CB719905, by the National Natural Science Foundation of China under Grants 61102128, 91338202 and 91338111, and in part by the Fundamental Research Funds for the Central Universities under Grant 211–274175.

References

[1] C. Hong, N. Li, M. Song, J. Bu, C. Chen, An efficient approach to content-based object retrieval in videos, Neurocomputing 74 (17) (2011) 3565–3575.
[2] Dimitris Manolakis, David Marden, Gary A. Shaw, Hyperspectral image processing for automatic target detection applications, Lincoln Lab. J. 14 (1) (2003) 79–116.
[3] C.-I. Chang, Target signature-constrained mixed pixel classification for hyperspectral imagery, IEEE Trans. Geosci. Remote Sens. 40 (5) (2002) 1065–1081.
[4] Q. Du, H. Ren, Real-time constrained linear discriminate analysis to target detection and classification in hyperspectral imagery, Pattern Recogn. 36 (1) (2003) 1–12.
[5] Hsuan Ren, Chein-I Chang, Automatic spectral target recognition in hyperspectral imagery, IEEE Trans. Aerosp. Electron. Syst. 39 (4) (2003) 1232–1249.
[6] Qian Du, I. Kopriva, Automated target detection and discrimination using constrained Kurtosis maximization, IEEE Geosci. Remote Sens. Lett. 5 (no.1) (2008) 38–42.
[7] D. Tao, X. Li, X. Wu, S.J. Maybank, General tensor discriminant analysis and gabor features for gait recognition, IEEE TPAMI 29 (10) (2007) 1700–1715. (Oct).

[8] D. Tao, X. Li, X. Wu, S.J. Maybank, Geometric mean for subspace selection, IEEE TPAMI 31 (2) (2009) 260–274.
[9] J. Yu, M. Wang, D. Tao, Adaptive hypergraph learning and its application in image classification, IEEE Trans. Image Process 21 (7) (2012) 3262–3272. (Jul).
[10] J. Yu, M. Wang, D. Tao, Semisupervised multiview distance metric learning for cartoon synthesis, IEEE Trans. Image Proces 21 (11) (2012) 4636–4648.
[11] D. Manolakis, C.h. Siracusa, G. Shaw, Hyperspectral subpixel target detection using the linear mixing model, IEEE Trans. Geosci. Remote Sens. 39 (7) (2001) 1392–1408.
[12] Joshua Broadwater, Rama Chellappa, Hybrid detectors for subpixel targets, IEEE Trans. Pattern Anal. 29 (11) (2007) 5713–5718.
[13] D. Manolakis, G. Shaw, Detection algorithms for hyperspectral imaging applications, IEEE Signal Process. Mag. 19 (1) (2002) 29–43.
[14] F. Vincent, O. Besson, C. Richard, matched subspace detection with hypothesis dependent noise power, IEEE Trans Signal Process 56 (11) (2008) 5713–5718.
[15] C. Gordon, A generalization of the maximum noise fraction transform, IEEE Trans. Geosci. Remote Sens. 38 (1) (2000) 608–610.
[16] A.A. Green, M. Berman, P. Switzer, M.D. Craig, A transformation for ordering multispectral data in terms of image quality with implications for noise removal, IEEE Trans. Geosci. Remote Sens. 26 (1988) 65–74.
[17] Y. Chen, N.M. Nasrabadi, T.D. Tran, Sparse representation for target detection in hyperspectral imagery, IEEE J. Select. Top. Signal Process. 5 (3) (2011) 629–640.
[18] T. Wang, B. Du, L. Zhang, A background self-learning framework for unstructured target detectors, IEEE Geosci. Remote Sens. Lett. 10 (6) (2013) 1577–1581.
[19] M.S. Stefanou, J.P. Kerekes, A method for assessing spectral image utility, IEEE Trans. Geosci. Remote Sens. 47 (6) (2009) 1698–1706.
[20] S.M. Schweizer, J.M.F. Moura, Efficient detection in hyperspectral imagery, IEEE Trans. Image Process. 10 (4) (2001) 584–597. (Apr).
[21] J. Davis and M. Goadrich, The relationship between Precision-Recall and ROC curves, in: Proceedings of the 23rd International Machine Learning, 2006, Pittsburgh, PA, 233–240.